

Spatially resolved small-angle neutron scattering in the 1-2 plane: A study of shear-induced phase-separating wormlike micelles

Matthew W. Liberatore, Florian Nettesheim, and Norman J. Wagner*

Department of Chemical Engineering, University of Delaware, Newark, Delaware 19716, USA

Lionel Porcar

University of Maryland, College Park, Maryland 20742, USA and NIST Center for Neutron Research, National Institute of Standards and Technology, Gaithersburg, Maryland 20899, USA

(Received 18 March 2005; published 27 February 2006)

The shear-induced microstructure of a shear-induced phase separating (SIPS) wormlike micellar solution is measured by combining small-angle neutron scattering with a shear cell capable of gap-resolved measurement in the 1-2 (velocity-velocity gradient) plane. Quantitative results show evidence for shear-induced microphase separation accompanied by shear banding. The results suggest both concentration fluctuations and gradients in segmental alignment occurring during SIPS.

DOI: [10.1103/PhysRevE.73.020504](https://doi.org/10.1103/PhysRevE.73.020504)

PACS number(s): 83.80.Qr, 81.16.Dn, 61.12.Ex, 83.50.Ax

The nonlinear rheological behavior of complex fluids includes rich phenomena such as shear-induced phase separation (SIPS). Although many polymeric and self-assembled systems show a wide variety of related phenomena, self-assembled solutions of surfactants forming wormlike micelles [1–3] have proven to be especially robust in exhibiting clear signatures of SIPS and as such, are a significant topic of scientific inquiry [4–13].

A rheological signature of SIPS in wormlike micelles is a stress plateau. Models suggest this corresponds to a multiphase flow regime composed of two bands at different shear rates with different micellar structures. While global rheological response is important in characterizing these wormlike micellar solutions, local velocity and concentration profiles provide a greater understanding of the phase separation and/or shear banding phenomenon. Rheo-optics can locate the critical shear rate for the onset of phase separation via turbidity, provide the average segmental alignment of the solution via flow-birefringence [2,10–12], as well as provide information about microphase separation through flow dichroism. Additionally, gap resolution using birefringence for shear-thickening surfactant solutions provide insight into the fluctuations of this flow-induced phenomenon [14]. Previous dynamic light scattering [9] and NMR [8] studies provide local velocity profiles of the shear banded state. More recently, particle tracking velocimetry [13] and ultrasound [15] provide spatial and temporal information about the kinetics of band formation in phase separating surfactant solutions. However, there is sparingly little information about the microstructure of the high shear band due to optical turbidity, and therefore, a small-angle neutron scattering (SANS) investigation in the flow-shear gradient plane is needed.

Previous studies using rheo-SANS quantified the average alignment by measuring the alignment factor in the flow-vorticity (1-3) plane [12]. Additional insight into the SIPS of wormlike micelles is gained by measuring in the shear

gradient-vorticity (2-3) plane and especially the flow-shear gradient (1-2) plane. Previous measurements in the 1-2 plane [16–18] were unable to resolve the possible existence of flow stratified regions of differing morphology. Here, we describe the first quantitative, gap-resolved SANS measurements in the 1-2 plane.

Model systems were formulated using the cationic surfactant erucyl bis(hydroxyethyl)methylammonium chloride (EHAC), $C_8H_{17}-CH=CH-C_{12}H_{24}-N(C_2H_4OH)_2CH_3$ (Akzo Nobel, Chicago, IL). Wormlike micelles were formed with hydrotropic salt, sodium salicylate (O-hydroxy benzoate, ACS-grade reagent, Sigma-Aldrich) in deuterium oxide (D_2O , Low Pa ramagnetic, Cambridge Isotope Laboratories). The sample used here, unless otherwise noted, is 40 mM (3.0 wt %) EHAC/300 mM (4.1 wt %) sodium salicylate in D_2O . The phase behavior and rheology of this system has been reported [12,19]. Microstructure studies indicate micellar branching in proximity to a two-phase region accessible at lower added salt concentrations.

Rheo-SANS measurements were conducted on the NG7 30 meter small-angle scattering instrument at the Center for Neutron Research at the National Institute of Standards and Technology (NIST) in Gaithersburg, Maryland. Measurements in the flow-vorticity (1-3) and shear gradient-vorticity (2-3) planes use the NIST Couette cell with aluminum cup (50 mm inner diameter) and quartz bob (48 mm diameter, 70 mm height) controlled by a UDS 200 rheometer (Paar Physica). The flow curve recorded during SANS experiments is within experimental error of previously reported values [12,19]. The flow-vorticity and shear gradient-vorticity data were recorded at $25 \pm 0.2 \text{ }^\circ\text{C}$. Detector distances of 4 and 15 m were used to cover a q range of 0.003 to 0.13 \AA^{-1} . At this q range the cross section of the micelles and their orientation are measurable.

Scattering patterns collected in the flow-shear gradient (1-2) plane employed a custom machined aluminum Couette (25 mm inner radius, 1.35 mm gap and 5 mm path length) sketched in Fig. 1 and described elsewhere in more detail [20]. A slit preceding the cell reduced the neutron beam to

*Electronic address: wagner@che.udel.edu

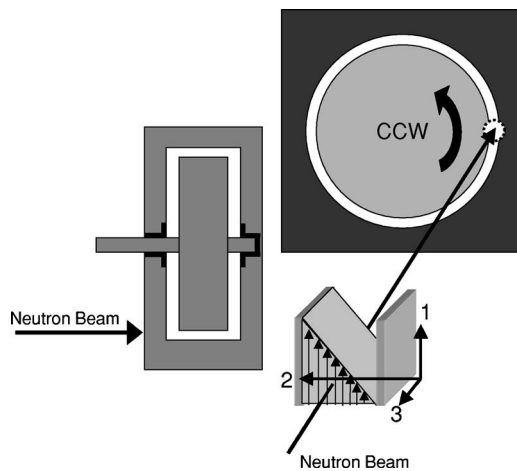


FIG. 1. Schematic of the 1-2 plane shear cell. Gap position is measured from the rotating inner wall to the stationary outer wall.

0.3 mm in width by 5.0 mm in height. The beam center was positioned at 0.2, 0.5, 0.8, and 1.2 mm from the inner (rotating) wall. A stepper motor was used to rotate the inner cylinder resulting in shear rates from 0.1 to 100 s⁻¹. Positive shear rates correspond to a counterclockwise rotation of the inner cylinder with respect to the path of the neutrons. Experiments were performed at $\lambda=6 \text{ \AA}$, $\Delta\lambda=22\%$, sample to detector distance of 4 and 15 m ($0.003 < q < 0.13 \text{ \AA}^{-1}$) at $24 \text{ }^\circ\text{C} \pm 0.5 \text{ }^\circ\text{C}$.

The sample of interest has been characterized by rheology, rheo-optics in the 1-2 plane as well as spatially resolved SANS. Figure 2 summarizes the condition of the sample under shear flow. In brief, the appearance of turbidity (i.e., low transmittance) corresponds with the stress plateau. Also, the magnitude of the flow birefringence grows with shear rate until the stress plateaus, indicating flow-induced segmental

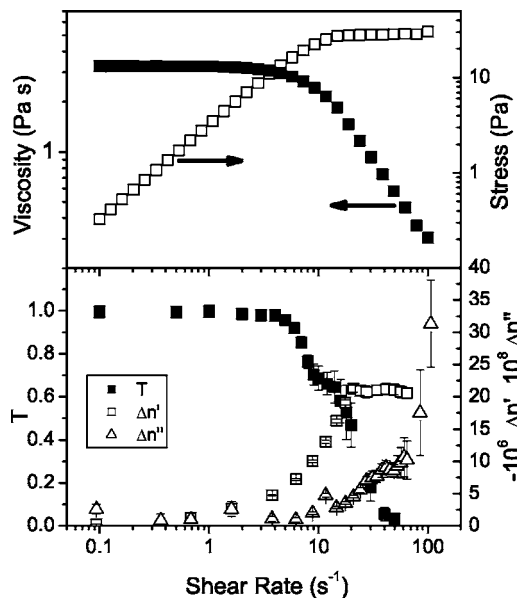


FIG. 2. Viscosity, stress, transmittance (T), birefringence ($\Delta n'$) and dichroism ($\Delta n''$) versus shear rate for 40 mM EHAC/300 mM NaSal/H₂O.

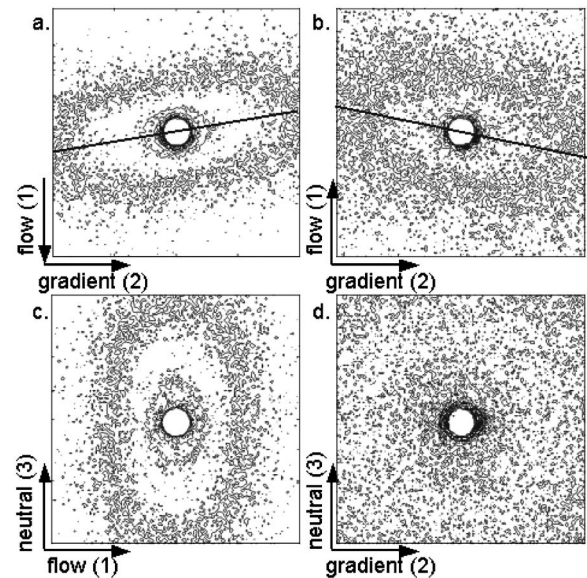


FIG. 3. 2D contour scattering patterns (a) in the 1-2 plane at $+32 \text{ s}^{-1}$ (90 m) (b) in the 1-2 plane at -32 s^{-1} (45 m) (c) in the 1-3 plane at 20 s^{-1} (d) in the 2-3 plane at 20 s^{-1} . The lines on (a) and (b) are drawn at their respective orientation angles, β .

alignment. Finally, dichroism indicates the formation of fluctuations in the refractive index oriented in the flow direction. The SANS observation will be put into context with the rheo-optical characterization presented in Fig. 2.

SANS patterns were collected in all three shear planes at rest and at shear rates spanning the Newtonian plateau through the shear thinning regime ($0.1 \leq \dot{\gamma} \leq 100 \text{ s}^{-1}$). An isotropic pattern is observed at rest and at shear rates below the onset of shear thinning ($\dot{\gamma} < 3 \text{ s}^{-1}$). Alignment, indicated by angular anisotropy in the two-dimensional (2D) scattering pattern, is evident for shear rates in the shear thinning regime (Fig. 3). Proper alignment and orientation of the cell with respect to the beam line is verified in Figs. 3(a) and 3(b), where shearing in opposite directions results in symmetry in the 1-2 SANS patterns about the flow direction. This alignment is also observed in the flow-vorticity plane [Fig. 3(c)] using the NIST Rheo-SANS cell, consistent with earlier findings [12]. Further, the shear gradient-vorticity contour in Fig. 3(d) is nearly isotropic as would be expected for weakly flow-aligned cylindrical micelles. Measurements in the 2-3 plane are complicated by the long path lengths and curvature of the sample geometry.

The alignment factor [21] as a function of shear rate for the 1-2 and 1-3 planes is shown in Fig. 4. In brief, $A_f=0$ corresponds to no net segmental alignment, while $A_f=-1$ represents complete flow alignment. Alignment factors in the 1-2 plane were obtained using a narrow slit providing gap resolution (partially filled circles), where 0 mm corresponds to the inner rotating cylinder. For the on-axis rheo-SANS experiments, $|A_f|_{1,3}$ evolves continuously from no alignment in the low shear plateau to significant segmental alignment in the shear thinning regime. The alignment in the 1-2 plane tracks these values, but shows that the alignment depends on the position within the gap at higher shear rates. Note that the alignment factors in the 1-3 plane will not, in general, be

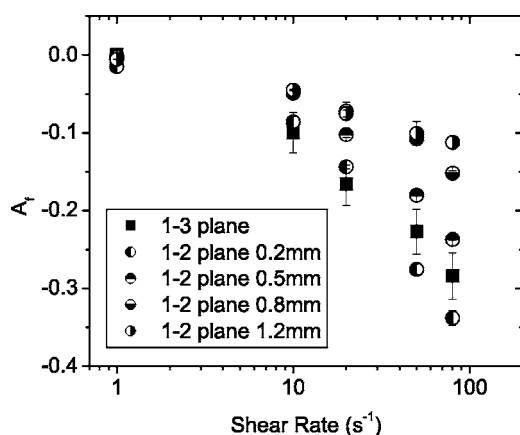


FIG. 4. Alignment factor as a function of shear rate in the 1-2 and 1-3 planes of flow. The gap position for the 1-2 plane data is indicated.

equal to those in the 1-2 plane; however, for flow-aligning systems with a director in the plane of shear, the two measurements are expected to be qualitatively similar. Nonetheless, the degree of segmental alignment is consistent with a flow-aligned dense, branched micellar network [12] and not a nematic phase of unbranched micelles as seen in other, non-SIPS but shear banding samples [11].

As seen in Fig. 5, the angle of the primary axis of alignment relative to the flow direction (β) decreases systematically with increasing shear rate. This orientation angle in the flow-shear gradient plane varies with the position across the gap. For reference, weak shearing is expected to induce alignment along the primary axis of strain (45°) while complete flow alignment corresponds to 0° . The greatest alignment is observed near the rotating inner cylinder at higher shear rates. These orientation angles correspond to those measured by flow birefringence.

Figure 5 shows that the alignment and orientation angle depend on position in the Couette cell gap. At lower nominal

shear rates, prior to SIPS ($\dot{\gamma} \leq 20 \text{ s}^{-1}$) this is expected simply due to the systematic increase in shear rate upon approaching the inner, rotating cylinder. Independent measurements of the local velocity gradients at these lower nominal shear rates confirm that the measured local orientation angles and alignment factors correspond to the expected values at the local shear rates. Velocimetry measurements indicate a very high local shear rate near the inner cylinder ($\dot{\gamma} > 300 \text{ s}^{-1}$) for the highest nominal shear rates. Strong turbidity and dichroism are observed at these high shear rates, and the sample is strongly phase separated. The region near the inner cylinder is striated and optically turbid, while the outer region remains optically clear, in agreement with other studies [13]. We propose that the inner band is a shear-induced phase separated material with coexisting phases, surfactant rich and surfactant lean, organized in the flow on length scales smaller than the width of the SANS beam (0.3 mm).

Further investigation into the scattering in the 1-2 plane provides insight into the shear-induced phase separation of the micellar solution. Strong scattering at low q values ($q < 0.0045 \text{ \AA}^{-1}$) with a q^{-4} scaling is indicative of interface scattering (i.e., Porod scattering), providing evidence for the SIPS phenomena at shear rates of 20 s^{-1} and above. A fit of the low q regime to a q^{-4} power law was obtained by subtracting the rod scattering from the data. The fit shown in Fig. 5(c) is a combination of the q^{-4} fit and the rod scattering. The crossover from q^{-4} to q^{-1} depends on the prefactor of the power law and thus, the specific area of the fluctuations formed under shear. Above 20 s^{-1} , two distinct bands are observed optically using particle tracking velocimetry (PTV) for this sample. Within the high shear band two phases apparently coexist with different surfactant concentration, which gives rise to the scattering contrast and q^{-4} profile. This is clear experimental evidence for the SIPS mechanism proposed in [12]. This sample is in proximity to a phase boundary, where thermodynamic phase separation leads to a viscous, flow-birefringent, surfactant rich phase in equilibrium with brine supernatant. Hence, we propose the observed

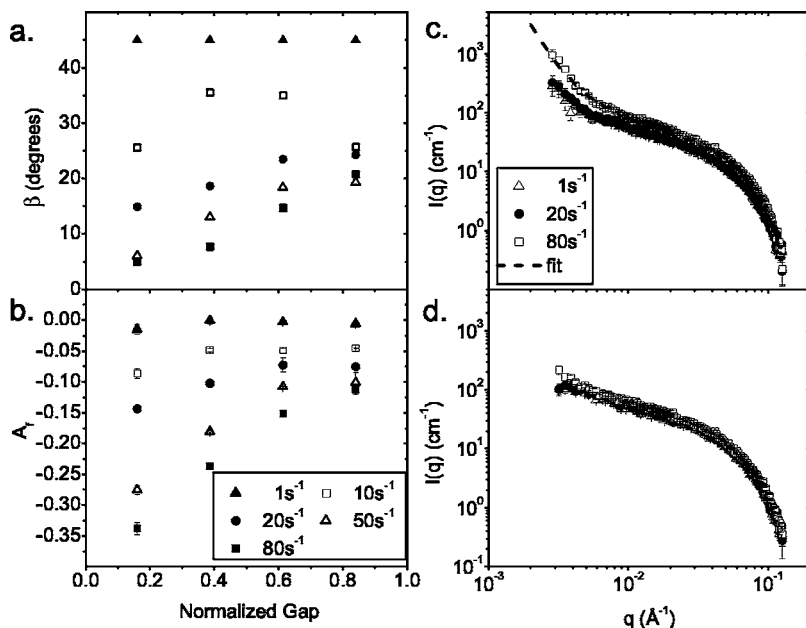


FIG. 5. Top left: The orientation angle β . Bottom left: Alignment factor measured in the 1-2 plane from the shear direction, is plotted as a function of gap position, measured from the inner, rotating cylinder, at various shear rates indicated by the symbols. Top right: Scattering profiles from the inner position (0.2 mm) at three different shear rates as indicated. The dashed line represents a combination of rod scattering and q^{-4} behavior fitted to the data. Bottom right: Scattering profiles at 0.8 mm from the inner cylinder at the same shear rates.

turbid striations in the high shear band are of similar composition, which is supported by the rheo-SANS data.

In summary, this wormlike micellar solution aligns under flow. A stress plateau is accompanied by turbidity and flow dichroism. New gap-resolved SANS measurements in the 1-2 plane show that the turbid band has a slightly higher alignment. This is proposed to be due to flow striation in micron sized shear bands composed of highly branched, concentrated micellar solution coexisting with a nearly isotropic, brine phase. This is in contrast to shear banding samples not exhibiting SIPS, which show a highly aligned, nematiclike state in the high shear band [11,13].

Theoretically, these two-fluid models [2,22–29] and the tube theory [3,30] predict shear banding, but up to now have not predicted average or gap-resolved alignment or orientation with respect to the flow. In most cases, these two-fluid models contain additional, usually phenomenological, terms,

which are added to the total stress, to obtain the shear banding phenomenon. Here, we connect the shear banding to the presence of an underlying thermodynamic phase separation. As surfactants self-assemble into a myriad of microstructures, models for shear banding in the wormlike surfactant solutions need to account for the possible existence of various mesophases in the high shear band coexisting with the low shear, branched wormlike micellar phase. Consequently, additional theoretical and experimental work is warranted to develop a physically realistic model for SIPS and shear banding in surfactant mesophases.

The authors wish to acknowledge the support of the NIST, U.S. Department of Commerce, in providing the neutron research facilities used in this work. Unilever and the Humboldt Stiftung (F.N.) are also acknowledged for providing financial support.

-
- [1] H. Rehage and H. Hoffmann, *Mol. Phys.* **74**, 933 (1991).
 [2] P. D. Olmsted, *Curr. Opin. Colloid Interface Sci.* **4**, 95 (1999) and references within.
 [3] N. A. Spenley, M. E. Cates, and T. C. B. McLeish, *Phys. Rev. Lett.* **71**, 939 (1993).
 [4] M. E. Cates, *J. Phys.: Condens. Matter* **8**, 9167 (1996).
 [5] P. Fischer, E. K. Wheeler, and G. G. Fuller, *Rheol. Acta* **41**, 35 (2002).
 [6] S. Fujii, T. Isojima, and K. Hamano, *Phys. Lett. A* **263**, 393 (1999).
 [7] M. Nowak, *Rheol. Acta* **37**, 336 (1998).
 [8] M. M. Britton and P. T. Callaghan, *Phys. Rev. Lett.* **78**, 4930 (1997).
 [9] J. B. Salmon, A. Colin, S. Manneville, and F. Molino, *Phys. Rev. Lett.* **90**, 228303 (2003).
 [10] S. Lerouge, J. P. Decruppe, and C. Humbert, *Phys. Rev. Lett.* **81**, 5457 (1998).
 [11] J. P. Decruppe, S. Lerouge, and J. F. Berret, *Phys. Rev. E* **63**, 022501 (2001).
 [12] B. A. Schubert *et al.*, *Langmuir* **20**, 3564 (2004).
 [13] Y. T. Hu and A. Lips, *J. Rheol.* **49**, 1001 (2005).
 [14] J. F. Berret, S. Lerouge, and J. P. Decruppe, *Langmuir* **18**, 7279 (2002).
 [15] V. Croce *et al.*, *Langmuir* **19**, 8536 (2003).
 [16] L. Noirez and A. Lapp, *Phys. Rev. Lett.* **78**, 70 (1997).
 [17] L. Noirez, *Phys. Rev. Lett.* **84**, 2164 (2000).
 [18] J. F. Berret, J. Vermant, and L. Noirez, in XIII International Congress on Rheology, Cambridge, UK, 2000 (unpublished), Vol. 3, p. 273.
 [19] S. R. Raghavan, H. Edlund, and E. W. Kaler, *Langmuir* **18**, 1056 (2002).
 [20] M. W. Liberatore *et al.* (unpublished).
 [21] L. M. Walker and N. J. Wagner, *Macromolecules* **29**, 2298 (1996).
 [22] C. Y. D. Lu, P. D. Olmsted, and R. C. Ball, *Phys. Rev. Lett.* **84**, 642 (2000).
 [23] X.-F. Yuan and L. Jupp, *Europhys. Lett.* **60**, 691 (2002).
 [24] J. K. G. Dhont, *Phys. Rev. E* **60**, 4534 (1999).
 [25] S. M. Fielding and P. D. Olmsted, *Phys. Rev. Lett.* **90**, 224501 (2003); **92**, 084502 (2004).
 [26] V. Schmitt, C. M. Marques, and F. Lequeux, *Phys. Rev. E* **52**, 4009 (1995).
 [27] F. Bautista *et al.*, *J. Non-Newtonian Fluid Mech.* **94**, 57 (2000).
 [28] G. Porte, J. F. Berret, and J. L. Harden, *J. Phys. II* **7**, 459 (1997).
 [29] L. P. Cook and L. F. Rossi, *J. Non-Newtonian Fluid Mech.* **116**, 347 (2004).
 [30] T. C. B. McLeish and R. C. Ball, *J. Polym. Sci., Polym. Phys. Ed.* **24**, 1735 (1986).